Micro-Doppler Signatures of Underwater Vehicles Using Acoustic Radar

Rajat Kashyap*, Inderdeep Singh* and Shobha Sundar Ram
Dept. of Electronics and Communications Engineering
Indraprastha Institute of Information Technology Delhi
Email: rajat12155@iiitd.ac.in, inderdeep12139@iiitd.ac.in, shobha@iiitd.ac.in

***Abstract*—Scattered radar returns from non-rigid moving bodies show distinct micro-Doppler features in the joint time-frequency space. As a result, Doppler spectrograms are useful feature vectors for identification and classification of aerial and ground based targets such as helicopters, humans and animals. In this paper, we present the micro-Doppler signatures of two underwater unmanned vehicles (UUV) from simulated acoustic radar data. The vehicles and radar are assumed to be fully submerged underwater. The radar scattered returns are generated using primitive based modeling of the vehicles at 30KHz. We consider two types of motions - vehicles move tangentially with respect to the radar and vehicles move radially towards the radar.**

I. Introduction

Detection and identification of underwater vehicles is an important component of security and surveillance operations along maritime borders. Several technologies, involving acoustic, video and lidar signals, have been explored in the past towards detecting underwater bodies [1]–[4]. Most of these technologies exploit the strength and Doppler of the backscattered data from the main body of the target to detect the target. However, most underwater vehicles are non-rigid bodies. Besides the translation motion of the main body of the target, components such as propellers, periscopes etc. undergo micro-motions (rotation, vibration and coning). The Doppler returns from non-rigid bodies are known to consist of micro-Doppler features arising from these micro-motions that are best visualized in the joint time-frequency space [5]. In this work, we propose to examine whether the micro-Doppler in the backscattered data can be used as a new feature vector for detection and identification of underwater vehicles. Due to the high attenuation of high frequency electromagnetic signals under water, we will generate the Doppler signatures using the scattered returns from continuous wave ultrasonic radar.

Over the last decade, Doppler based sensing has emerged as an effective tool towards tracking and monitoring non-rigid ground based and aerial targets [6]–[14]. There have been extensive research carried out by the radar community to exploit the micro-Doppler features to detect and classify different types of human motions such as walking, running and crawling [15]. The swinging motions of the human arms and legs in each of these motions gives rise to distinct micro-Doppler patterns in the joint time-frequency space with respect to the Doppler arising from the translational motion of the torso. The signatures of bipedal humans are also quite distinct from the signatures of quadruped animal motions or the motions of inanimate objects [16]. Similarly, the radar signatures of aerial targets such as helicopters and ground based vehicles are also characterized by distinct features suitable for detection [17], [18]. For instance, the moving blades of helicopters and rotating wheels of ground based vehicles give rise to distinct micro-Doppler signatures that form robust feature vectors for classification. Narrowband Doppler sensors offer several advantages compared to wideband radar sensors - narrowband sensors can usually be manufactured from cheap off-the-shelf components [7]; they are quite robust to multipath effects in complex propagation environments [10]; background noise from stationary clutter is automatically suppressed without the requirement of complex signal processing algorithms. The main limitations are that the signatures are quite different from conventional radar images of targets generated with wideband waveforms. The Doppler signatures are usually unintuitive to radar operators and therefore difficult to interpret.

Micro-Doppler signatures of acoustic radar signals have been generated in the past for human targets [19], [20]. Acoustic radar signals get much less attenuated through metal walls compared to microwave radar signals. In this work, we will simulate the acoustic micro-Doppler signatures of two underwater vehicles when both the radar and vehicle are submerged below water. The radar cross-sections of complex targets can be simulated using two different techniques. The first technique involves considering the vehicle as a complex target composed of multiple primitives of known cross-section areas, each with unique point scatterers. This technique is simple to implement and can be rapidly extended to model the scattered returns of moving targets across multiple time frames. Alternately, computational modeling techniques (such as finite element methods) can be used to generate very accurate radar cross-sections. In our work, we propose to use the primitive-based modeling technique over the computational techniques for the following reasons - (1) Computational techniques are unsuitable for generating the time-varying radar cross-sections of non-rigid bodies due to the computational cost of generating the RCS for each time frame of data; (2) Primitive based models have proven to be successful in generating the micro-Doppler signatures of a wide variety of targets (humans, animals, ground vehicles, helicopters etc.).

*Both authors have contributed equally to the work.

978-1-4799-8232-5/151$31.00@2015IEEE

In our paper, the micro-Doppler components arise from the rotation of the propellers blades on the body of the vehicle. The signatures are generated for both radial and tangential motions of the vehicles with respect to a radar. The paper is organized as follows. In the following section, we present the methodology to simulate the micro-Doppler signatures of the underwater vehicles using primitive based modeling techniques. In section III, we present the micro-Doppler signatures for two different motions of two vehicles. The micro-Doppler features arising from different components of the non-rigid body are identified for each case and the feasibility of using the Doppler spectrograms as feature vectors for identification and classification of the vehicles is discussed.

II. Primitive Based Modeling of Underwater Vehicles

In this section, we describe the primitive-based method used to model the micro-Doppler signatures of underwater vehicles. The primitive based model has been successfully used previously to model several complex radar targets such as humans, animals, helicopters and ground vehicles. In [19], primitive based techniques were used to model the acoustic micro-Doppler signatures of humans. It is computationally much simpler than other methods used for generating radar cross-sections of complex targets such as finite element method (FEM) and complex ray tracing. FEM is specifically unsuited for this problem, since the micro-Doppler signatures are generated from time-varying radar returns. Therefore, the computation of the radar cross-section of the target has to be repeated for each time frame. We model an underwater unmanned vehicle (UUV) as a complex target consisting of a combination of primitives such as cones, ellipsoids, cylinders and spheres. The radar cross-section of each of these primitives is well known [21], [22]. We assume a monostatic acoustic radar operating with a continuous wave source of λ wavelength. Both the radar and the target are submerged under water. The depth of the target and radar from the surface of the water and their respective heights from seafloor are assumed to be much greater than the distance between the target and the radar. Therefore multipath components caused due to reflections from the water-air interface and from the floor are neglected. The time domain scattered returns, $s(t)$, at the radar are given by the complex sum of the returns from each primitive, b, constituting the complex target as shown in (1).

$$s(t) = \sum_{b} \frac{\Gamma \sqrt{\sigma_b(\theta_b, \phi_b)}}{r_b^2} e^{-2j(\beta - j\alpha) r_b} \tag{1}$$

Here, Γ is the reflection coefficient of the acoustic signal from the surface of the UUV; σ_b is the radar cross-section of each primitive and therefore a function of the orientation of the primitive with respect to the radar; r_b is the distance between the phase center on the primitive and the radar; $\beta = \frac{2\Pi}{\lambda}$ and α are the propagation constant and attenuation constant of the acoustic signal in water. As the target moves, the position, (r_b, θ_b, ϕ_b), of the phase center and the RCS of each primitive will change. The phase center is estimated analytically by identifying a point on the surface of the primitive with the shortest distance from the radar. The reflection coefficient is computed for normal incidence of the radar signal from water to the UUV material. The attenuation constant is a function of the depth of the radar from the surface of the water, the temperature of the water, the signal frequency and the salinity of the water [23]. Some of the key assumptions of this model are: (1) Multiple and higher order interactions between different primitives are not considered in this model; (2) Shadowing of some of the parts of the target from the radar are also not considered in this model. The joint time-frequency representation of the radar data is generated by the application of the short-time Fourier transform on the time-domain data.

$$\chi(f,t) = \int s(\tau) h(t-\tau) e^{-j2\pi f \tau} d\tau \tag{2}$$

Here, $h(t)$ is the short time window that is applied on the time-domain data.

III. Simulation of Micro-Doppler Signatures Using Acoustic Radar Data

In this section, we present the micro-Doppler signatures of two UUVs for different orientations of the target motion with respect to the radar. The first UUV model is a light autonomous underwater vehicle (LAUV) developed by Laboratory for Underwater Systems and Technologies (LSTS), Portugal [24] as shown in Fig.1(a). We generated a computer aided design (CAD) model capturing the key features of the UUV, in MATLAB, based on design specifications detailed in Fig.1(b) and Table I. The UUV undergoes a translational motion at a velocity of $[2.5, 0, 0]m/s$ or $4.86knots$ along the X axis. The center of the UUV moves from $[50, 0, 0]m$ to $[57.5, 0, 0]m$. The three propellers rotate at an angular velocity of $120rpm$. We assume that a monostatic acoustic radar operates at $30KHz$ and $0dBm$ and is located at $[53, 0, 10]$ as shown in Fig.1(c). The sampling frequency is chosen to be $1kHz$ to satisfy Nyquist conditions. We consider the UUV to be a complex target consisting of multiple primitives such as cylinders, cones and ellipsoids as shown in Fig.1(b). For instance, the central part of the main body and several of the other components of the UUV are modeled as cylinders, whose RCS is given by

$$\sigma_{CYL} = \frac{\lambda r sin\theta}{8\pi (cos\theta)^2} \quad \forall \ \theta \neq 90^\circ \tag{3}$$

$$\sigma_{CYL} = \frac{2\pi H^2 r}{\lambda}, \ \ \theta = 90^\circ \tag{4}$$

Here θ is the angle between the long axis of the cylinder and the line-of-sight vector between the center of the cylinder and the radar; r & H are the radius and height of the cylinder respectively. The rear end of the UUV is capped by a cone whose RCS is calculated using the RCS of frustum

$$\sigma_{FRUSTUM} = \frac{\lambda z_1 tan\delta}{8\pi \sin\theta} \left[\tan(\theta + \delta)\right]^2 \tag{5}$$

$$z_1 = \frac{r1}{\tan\delta} \tag{6}$$

where δ is the half cone angle calculated using (7)

$$\tan\delta = \frac{r_2 - r_1}{H_1} \tag{7}$$

Here, r_1 and r_2 are the minor and major radii of the frustum respectively. For calculating the RCS of a cone we assumed r_1 to be negligibly small. H_1 is the height of the frustum and θ is the angle between the height vector of the cone and the radar LOS vector. The RCS of the hemisphere at the front of the UUV is given by

$$\begin{aligned}\sigma = 4\pi\lambda^2 \Bigg| & \frac{e^{j2\beta a}}{4\beta}\left[(1-j2\beta a)(1-je^{-j2\beta d}) - j2\beta d e^{-j2\beta d}\right] \\ & - j\frac{\rho}{n} sin\left(\frac{\pi}{n}\right) cos\left(\theta\right) e^{j2\beta(a-d)} \\ & \left(cos\left(\frac{\pi}{n}\right) - cos\left(\frac{3\pi}{n}\right)\right)^{-1}\Bigg|^2\end{aligned} \tag{8}$$

where

$$n = \frac{3}{2} + \frac{\theta}{\pi} \tag{9}$$

$$\theta = sin^{-1}\left(\tfrac{a-d}{a}\right) \tag{10}$$

$$\rho = (a^2 - (a-d)^2)^{1/2} \tag{11}$$

Here a and d are equal to the radius and the depth of the hemisphere respectively. These two will be equal for a perfect hemisphere. The propellers are modeled as ellipsoids. The RCS of an ellipsoid is given by

$$\sigma_{El} = \frac{\pi a^2 b^2 c^2}{((a^2\sin^2\theta\cos^2\phi)+(b^2\sin^2\theta\sin^2\phi)+(c^2\cos^2\theta))^2} \tag{12}$$

where θ and ϕ are the elevation and azimuth angles respectively and a, b, c are the semi axes of the ellipsoid. For each of the primitives, a unique phase center is identified as that point on the surface of the primitive where the incident vector is coincident with the surface normal vector. The UUV is assumed to be made of HY80 alloy and is entirely submerged under water. Therefore, the reflection coefficient of an acoustic signal for normal incidence is given by $\Gamma = \frac{z_2 - z_1}{z_2 + z_1}$ where z_2 and z_1 are the acoustic impedances of HY80 and water respectively. They are $4.2627 \times 10^7 rayls$ and $1.5866 \times 10^6 rayls$. If the temperature of sea water is $30.72°C$, the salinity of the water is $35ppt$, depth of radar is $50m$ and pH of the water is 8, the attenuation coefficient of the sound in water at $30kHz$ is $3.476dB/km$ [23]. The short-time Fourier transform (STFT) is applied on the time-domain data using a short time window of $0.13s$. The choice of the short time window is dictated by optimum time and frequency resolution of the resultant Doppler spectrogram shown in Fig.2. The spectrogram clearly indicates two components - a strong Doppler component arising from the translational motion of the main body of the UUV (as shown in Fig.2(b)) as well as weaker micro-Doppler components due to the rotation of the three propellers (as shown in Fig.2(a)). As the UUV moves along a straight path before the radar, the Doppler is initially positive as the target moves towards the radar, and then becomes negative as the target moves away from the radar. The strong return at the time instant of 1 second is because the UUV is directly before the radar at position $[53, 0, 0]m$. The Doppler is close to zero but the RCS of the cylindrical body is very high (4). This gives rise to an impulse in the time-domain returns and thereby a Doppler spread in the frequency domain. The propellers rotate at an angular velocity of $120rpm$, and hence the Dopplers show a periodicity of $0.5s$. As the blades approach the radar, the Dopplers are positive and the Dopplers become negative as they move away from the radar. Due to the smaller size of propellers in comparison to the size of the main body of the UUV, the RCS of the propellers is significantly lower. Next, we consider the case of the LAUV moving radially towards the radar from an initial position of $[65, 0, 0]$, as shown in Fig.1(d). The micro-Doppler signature of the radar returns are shown in Fig.2(d). Here we do not see the unique micro-Doppler features due to the propeller blades because the motion of the blades is mostly tangential with respect to the radar. The two results clearly indicate that the micro-Doppler features can be quite weak in comparison to the returns from the main body. Also, the orientation of the motion of the target with respect to the radar is quite critical in determining the nature of the resulting spectrogram. Next, we considered a second UUV, the HUGIN1000, from the HUGIN family of UUVs developed by Kongsberg Maritime, Norway as shown in Fig.3(a). Again, we generated a CAD model capturing the key features of HUGIN1000 in MATLAB. The dimensions of the different components of this model are presented in the Fig.3(b) and Table II. Note that the propellers of the HUGIN1000 are approximately 4.8 times longer than the propellers of the LAUV. In order to compare the micro-Doppler signatures of the HUGIN1000 with the LAUV, we retained the same set of position and velocity parameters for the radar and the target as the previous cases with the LAUV. The HUGIN1000 is modeled as a complex target consisting of different primitives as shown in Fig.3(b). The micro-Doppler returns from the three rotating propeller blades obtained for HUGIN1000 are shown in Fig.4(a). Again, the periodicity of the micro-Doppler features is $0.5s$. However, due to longer length of the blades in comparison to the previous case, the Dopplers reach a peak to peak value of around $300Hz$ in comparison to $60Hz$ in the case of LAUV. In other words, the micro-Doppler of the propeller blades are directly proportional to the length of the blades. The Doppler returns from the main body are shown in Fig.4(b). We see no micro Doppler due to the absence of any micro-motion. The radar signal is normally incident on the body of the target at time instants of 1 second and 2 seconds. The combined radar returns from the body and from the propeller blades are shown in Fig.4(c). In this case too, the magnitude of micro-Doppler returns due to the rotation of propeller blades is much weaker than the Doppler returns from the main body due to the small size of the propellers. Yet, the micro-Doppler gives us important information regarding the size of the propeller and the speed at which it rotates. Next, we consider a different orientation of the target with respect to the radar as shown in Fig.3(d). Here, the main body of the target is moving radially with respect to the

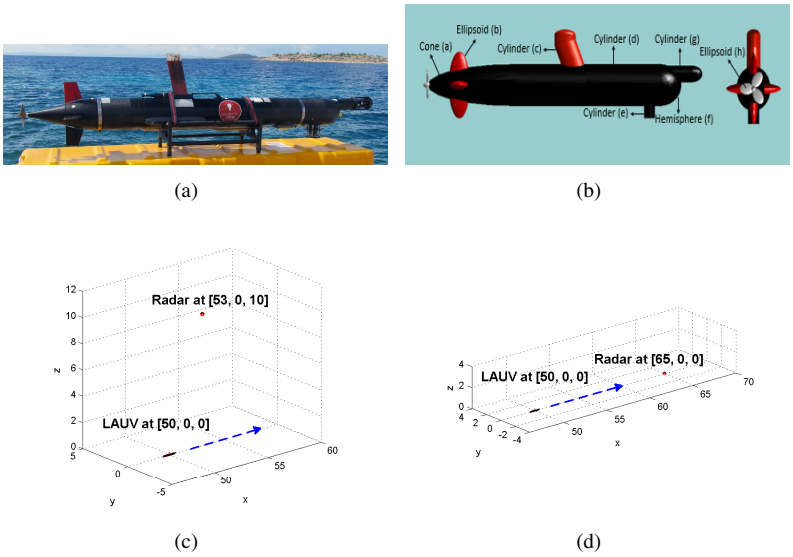

(a) (b)

(c) (d)

Fig. 1. (a) Light Autonomous underwater Vehicle(LAUV) obtained from [24], (b) CAD model of LAUV generated using MATLAB, (c) Animation model of motion of target along a straight path in front of the radar such that motion is tangential with respect to line-of-sight when target is directly before the radar, (d) Animation model of motion of target in a radial direction towards the radar

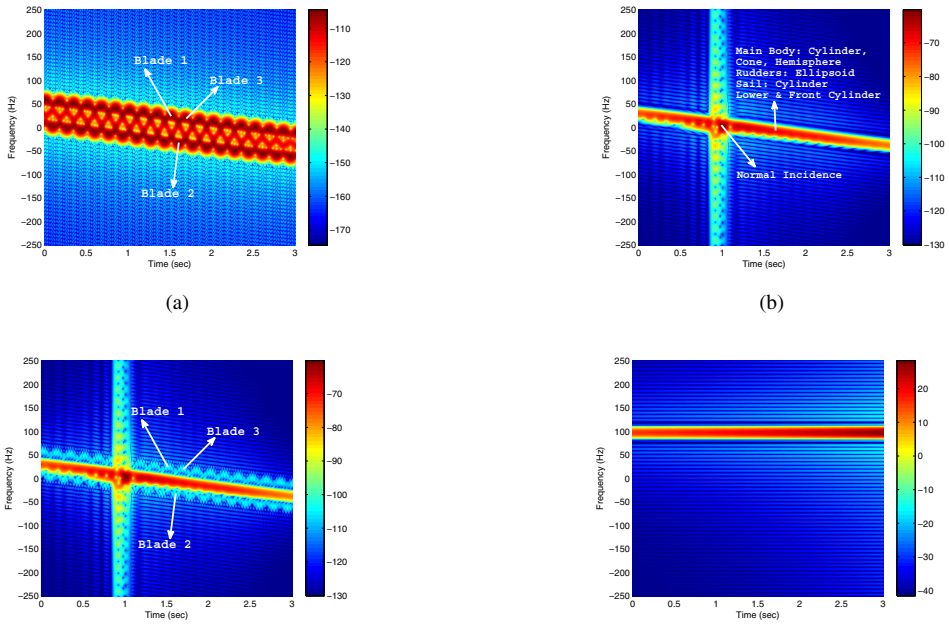

(a) (b)

(c) (d)

Fig. 2. Micro-Doppler signatures for LAUV while considering the scattered returns from (a) propeller blades (b) the rest of the main body except for the blades and (c) the entire target when target is moving as described in Fig.1(c). (d) Micro-Doppler signatures while considering the scattered returns from the entire target when target is moving as described in Fig.1(d).

S.No.	Primitives	Dimensions (meters)
1	Cone (a)	Height: 0.2391, Radius: 0.0750
2	Ellipsoid (b)	Major Axis: 0.1413, Minor Axis: 0.0327, 0.01
3	Cylinder (c)	Height: 0.2019, Radius: 0.0522
4	Cylinder (d)	Height: 0.6521, Radius: 0.0750
5	Cylinder (e)	Height: 0.0749, Radius: 0.0340
6	Hemisphere (f)	Radius: 0.0750
7	Cylinder (g)	Height: 0.1383, Radius: 0.0346
8	Ellipsoid (h)	Major Axis: 0.030, Minor Axis: 0.0200, 0.0050

TABLE I
DIMENSIONS OF CAD MODEL OF LAUV

S.No.	Primitives	Dimensions (meters)
1	Ellipsoid (a)	Major Axis: 1.920, Minor Axis: 0.3750, 0.3750
2	Cylinder (b)	Height: 0.6600, Radius: 0.0900
3	Ellipsoid (c)	Major Axis: 0.1350, Minor Axis: 0.3000, 0.0300
4	Ellipsoid (d)	Major Axis: 0.1450, Minor Axis: 0.0600, 0.0050

TABLE II
DIMENSIONS OF CAD MODEL OF HUGIN1000

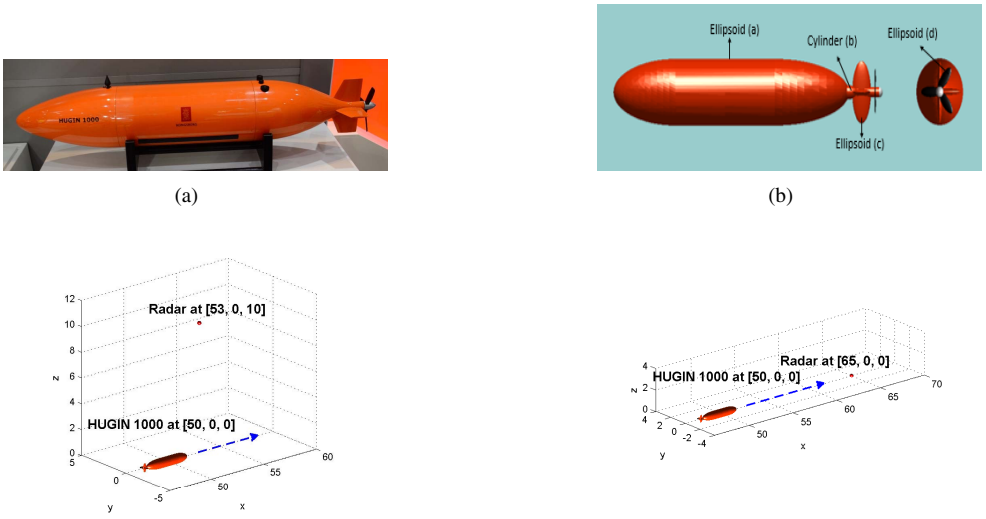

(a) (b) (c) (d)

Fig. 3. (a) Underwater vehicle HUGIN1000 from [24], (b) CAD model of HUGIN1000 generated using MATLAB, (c) Animation model of motion of target along a straight path in front of the radar such that motion is tangential with respect to line-of-sight when target is directly before the radar, (d) Animation model of motion of target in a radial direction towards the radar

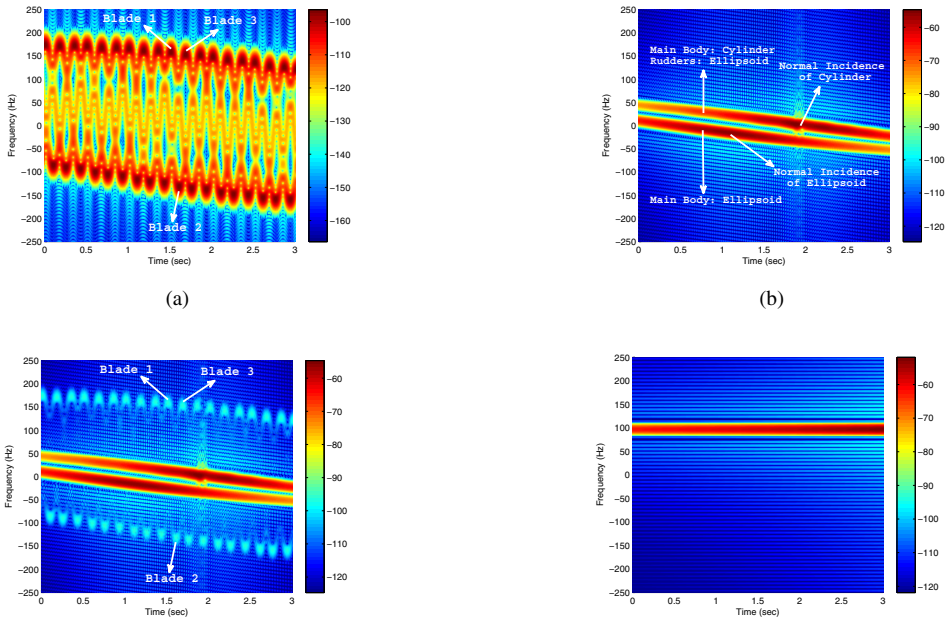

(a) (b) (c) (d)

Fig. 4. Micro-Doppler signatures for HUGIN1000 while considering the scattered returns from (a) propeller blades (b) the rest of the main body except for the blades and (c) the entire target when target is moving as described in Fig.3(c). (d) Micro-Doppler signatures while considering the scattered returns from the entire target when target is moving as described in Fig.3(d).

radar. Therefore, the Doppler from the main body is positive, in Fig.4(d), and greater in magnitude than the previous case shown in Fig.4(b). However, since the motion of the propellers is mostly tangentially with respect to the radar, we are unable to discern any micro-Doppler.

IV. Conclusion

Micro-motions of some parts of a moving underwater vehicle, such as rotating blades, give rise to interesting micro-Doppler features in the Doppler spectrograms of the scattered acoustic radar data. Preliminary results suggest that different UUVs show unique micro-Doppler features that are a function of the length of the propeller blades, their rotation rate as well as the orientation of the target motion with respect to the radar. More detailed studies have to be under taken to investigate the impact of more complex propagation mediums (multipath from the sea floor and the air-water interface; presence of obstructions along the line-of-sight between target and radar; presence of other sources of interferences etc.) have to be conducted before the robustness of the micro-Doppler feature vectors can be estimated.

Acknowledgment

This work is supported by the DST Inspire Faculty Fellowship granted by the Department of Science and Technology, Govt. of India.

References

[1] H. Fujimoto, T. Hamada, T. Hayashi, Y. Hiraoka, G. Mori, Y. Tominaga, and Y. Yoshida, "Underwater detection system," Sep. 8 1998, uS Patent 5,805,528.

[2] D. Walther, D. Edgington, and C. Koch, "Detection and tracking of objects in underwater video," in *Computer Vision and Pattern Recognition, 2004. Proceedings of the 2004 IEEE Computer Society Conference*, vol. 1. IEEE, 2004, pp. 1–4.

[3] J. J. Holmes and J. F. Scarzello, "Underwater detection and deterrent system," Jul. 20 2004, uS Patent 6,765,487.

[4] L. Raillon, J.-J. Fyot, R. Quer, and C. Debaillon-Vesque, "Towed low-frequency underwater detection system," May 31 2005, uS Patent 6,901,029.

[5] V. C. Chen, F. Li, S.-S. Ho, and H. Wechsler, "Micro-doppler effect in radar: phenomenon, model, and simulation study," *Aerospace and Electronic Systems, IEEE Transactions on*, vol. 42, no. 1, pp. 2–21, 2006.

[6] G. E. Smith, K. Woodbridge, and C. Baker, "Template based micro-doppler signature classification," in *High Resolution Imaging and Target Classification, 2006. The Institution of Engineering and Technology Seminar on*. IET, 2006, pp. 127–144.

[7] A. Lin and H. Ling, "Frontal imaging of human using three-element doppler and direction-of-arrival radar," *Electronics Letters*, vol. 42, no. 11, pp. 660–661, 2006.

[8] I. Bilik, J. Tabrikian, and A. Cohen, "GMM-based target classification for ground surveillance doppler radar," *Aerospace and Electronic Systems, IEEE Transactions on*, vol. 42, no. 1, pp. 267–278, 2006.

[9] P. Setlur, M. Amin, and F. Ahmad, "Urban target classifications using time-frequency micro-doppler signatures," in *Signal Processing and Its Applications, 2007. ISSPA 2007. 9th International Symposium on*. IEEE, 2007, pp. 1–4.

[10] S. S. Ram, Y. Li, A. Lin, and H. Ling, "Doppler-based detection and tracking of humans in indoor environments," *Journal of the Franklin Institute*, vol. 345, no. 6, pp. 679–699, 2008.

[11] N. Maaref, P. Millot, C. Pichot, and O. Picon, "A study of UWB FM-CW radar for the detection of human beings in motion inside a building," *Geoscience and Remote Sensing, IEEE Transactions on*, vol. 47, no. 5, pp. 1297–1300, 2009.

[12] V. Chen, G. Smith, K. Woodbridge, and C. Baker, *Through-the-wall radar imaging*. CRC press, 2010, no. 15.

[13] G. E. Smith and B. G. Mobasseri, "Robust through-the-wall radar image classification using a target-model alignment procedure," *Image Processing, IEEE Transactions on*, vol. 21, no. 2, pp. 754–767, 2012.

[14] J. Bryan, J. Kwon, N. Lee, and Y. Kim, "Application of ultra-wide band radar for classification of human activities," *IET Radar, Sonar & Navigation*, vol. 6, no. 3, pp. 172–179, 2012.

[15] Y. Kim and H. Ling, "Human activity classification based on micro-doppler signatures using a support vector machine," *Geoscience and Remote Sensing, IEEE Transactions on*, vol. 47, no. 5, pp. 1328–1337, 2009.

[16] H. Ling *et al.*, "Microdoppler signature simulation of computer animated human and animal motions," in *2008 IEEE Antennas and Propagation Society International Symposium*, 2008, pp. 1–4.

[17] T. Thayaparan, S. Abrol, E. Riseborough, L. Stankovic, D. Lamothe, and G. Duff, "Analysis of radar micro-doppler signatures from experimental helicopter and human data," *IET Radar, Sonar & Navigation*, vol. 1, no. 4, pp. 289–299, 2007.

[18] A. Ghaleb, L. Vignaud, and J. Nicolas, "Micro-doppler analysis of wheels and pedestrians in ISAR imaging," *Signal Processing, IET*, vol. 2, no. 3, pp. 301–311, 2008.

[19] Z. Zhang, P. O. Pouliquen, A. Waxman, and A. G. Andreou, "Acoustic micro-doppler radar for human gait imaging," *The Journal of the Acoustical Society of America*, vol. 121, no. 3, pp. EL110–EL113, 2007.

[20] K. Kalgaonkar and B. Raj, "Acoustic doppler sonar for gait recogination," in *Advanced Video and Signal Based Surveillance, 2007. AVSS 2007. IEEE Conference on*. IEEE, 2007, pp. 27–32.

[21] B. R. Mahafza, *Radar systems analysis and design using MATLAB*. CRC press, 2000.

[22] E. F. Knott, J. Shaeffer, and M. Tuley, *Radar cross section*. SciTech Publishing, 2004.

[23] M. A. Ainslie and J. G. McColm, "A simplified formula for viscous and chemical absorption in sea water," *The Journal of the Acoustical Society of America*, vol. 103, no. 3, pp. 1671–1672, 1998.

[24] (2013) Light autonomous underwater vehicle. Dep. de Eng. Electrotcnica e de Computadores. Porto, Portugal. [Online]. Available: http://lsts.pt/vehicles/lauv